

# The nuclear matter equation of state with consistent two- and three-body perturbative chiral interactions

L. Coraggio,<sup>1</sup> J. W. Holt,<sup>2</sup> N. Itaco,<sup>1,3</sup> R. Machleidt,<sup>4</sup> L. E. Marcucci,<sup>5,6</sup> and F. Sammarruca<sup>4</sup>

<sup>1</sup>*Istituto Nazionale di Fisica Nucleare,*

*Complesso Universitario di Monte S. Angelo, Via Cintia - I-80126 Napoli, Italy*

<sup>2</sup>*Physics Department, University of Washington, Seattle, WA 98195, USA*

<sup>3</sup>*Dipartimento di Fisica, Università di Napoli Federico II,*

*Complesso Universitario di Monte S. Angelo, Via Cintia - I-80126 Napoli, Italy*

<sup>4</sup>*Department of Physics, University of Idaho, Moscow, ID 83844, USA*

<sup>5</sup>*Dipartimento di Fisica “Enrico Fermi”, Università di Pisa, Largo Bruno Pontecorvo 3 - I-56127 Pisa, Italy*

<sup>6</sup>*Istituto Nazionale di Fisica Nucleare, Sezione di Pisa,*

*Largo Bruno Pontecorvo 3 - I-56127 Pisa, Italy*

(Dated: July 2, 2021)

We compute the energy per particle of infinite symmetric nuclear matter from chiral  $N^3\text{LO}$  (next-to-next-to-next-to-leading order) two-body potentials plus  $N^2\text{LO}$  three-body forces. The low-energy constants of the chiral three-nucleon force that cannot be constrained by two-body observables are fitted to reproduce the triton binding energy and the  ${}^3\text{H}$ - ${}^3\text{He}$  Gamow-Teller transition matrix element. In this way, the saturation properties of nuclear matter are reproduced in a parameter-free approach. The equation of state is computed up to third order in many-body perturbation theory, with special emphasis on the role of the third-order particle-hole diagram. The dependence of these results on the cutoff scale and regulator function is studied. We find that the inclusion of three-nucleon forces consistent with the applied two-nucleon interaction leads to a reduced dependence on the choice of the regulator only for lower values of the cutoff.

PACS numbers: 21.30.Fe, 21.65.Cd, 21.60.Jz

## I. INTRODUCTION

High-precision nuclear potentials based on chiral perturbation theory (ChPT) [1–3] are nowadays widely employed to link the fundamental theory of strong interactions, quantum chromodynamics (QCD), to nuclear many-body phenomena. An important feature of ChPT is that nuclear two-body forces, many-body forces, and currents [3–5] are generated on an equal footing. Consistency then requires that certain low-energy constants (LECs) appearing in the two-nucleon-force (2NF) — and fitted to two-nucleon data — appear also in three-nucleon forces (3NF), four-nucleon forces (4NF), and electroweak currents.

Since ChPT is a low-momentum expansion valid only for momenta  $Q < \Lambda_\chi \simeq 1$  GeV, where  $\Lambda_\chi$  denotes the chiral symmetry breaking scale, nucleon-nucleon ( $NN$ ) potentials derived from ChPT are typically multiplied by a (non-local) regulator function

$$f(p', p) = \exp[-(p'/\Lambda)^{2n} - (p/\Lambda)^{2n}], \quad (1)$$

where  $\Lambda \simeq 0.5$  GeV is a typical choice for the cutoff scale. In the effective field theory (EFT) framework, the calculated physical observables ideally will be independent of both the regulator function and the associated cutoff scale  $\Lambda$ . In the case of nuclear interactions this is rarely the case, and varying the regulator is often used as a tool to estimate the uncertainty in the theoretical calculations. In the two-nucleon problem, the dependence of the solutions of the Lippmann-Schwinger equation on the regulator function and its cutoff scale is minimized

by a renormalization procedure in which the LECs associated with  $NN$  and  $\pi N$  vertices are readjusted to two-nucleon phase shifts and deuteron properties. Even though potentials with different regulator functions yield similar phase shifts, they will in general give different predictions when employed in many-body calculations, due to their different off-shell behavior. One is then faced with a larger cutoff dependence in many-body systems [6], which should be reduced by a consistent adjustment of the LECs appearing in nuclear many-body forces.

In a recent paper [7], we have studied the regulator dependence of the cold neutron matter equation of state (EOS) employing chiral two- and three-nucleon potentials within many-body perturbation theory. Previous studies of infinite symmetric nuclear matter and pure neutron matter [8–16] have focused on the importance of nuclear many-body forces and have explored the perturbative and non-perturbative features of chiral nuclear potentials. In Ref. [7] we observed that in neutron matter calculations the use of consistent 3NFs plays a crucial role in the restoration of regulator independence. The calculation of the ground state energy of infinite neutron matter with chiral 3NFs up to  $N^2\text{LO}$  depends only on LECs that have been fixed in the two-nucleon system [17]. In the case of symmetric nuclear matter, also the one-pion exchange three-nucleon force  $V_{3N}^{1\pi}$  and the contact three-nucleon force  $V_{3N}^{\text{cont}}$  at  $N^2\text{LO}$  contribute. Therefore, the associated LECs  $c_D$  and  $c_E$ , which are not constrained by two-body observables, must also be refitted for different regulator functions. These 3NF LECs should be adjusted to  $A = 3$  observables only, and a possible choice [18–20]

is to reproduce the  ${}^3\text{H}$  and  ${}^3\text{He}$  binding energies together with the triton half-life (specifically the Gamow-Teller matrix element).

In the present work, we continue the investigation started in Ref. [7] and study the dependence of the EOS of symmetric nuclear matter on the choice of regulator function in the chiral nuclear potentials, employing two- and three-nucleon forces with consistent LECs. The ability to obtain realistic nuclear matter predictions with (consistent) two- and three-body interactions constrained by the properties of the two- and the three-nucleon systems and no additional adjustments is a focal point of this paper. Historically, this has proven to be a non-trivial task. As in Ref. [7], we employ three different chiral potentials with cutoff scales  $\Lambda = 414$  MeV [21], 450 MeV, and 500 MeV [1, 3]. The LECs  $c_D$  and  $c_E$  of the  $\text{N}^2\text{LO}$  chiral three-nucleon force are fitted, for each value of  $\Lambda$ , to the binding energies of  $A = 3$  nuclei and the  ${}^3\text{H}$ - ${}^3\text{He}$  Gamow-Teller matrix element. Note that the  $\Lambda = 500$  MeV two- and three-nucleon chiral potentials have been used to study  $A = 3$  and 4 elastic scattering [22], the  $A \leq 3$  nuclei electromagnetic structure [23] and low energy reactions of astrophysical interest [24], finding good agreement with the experimental data when available.

We compute the energy per particle of symmetric nuclear matter up to third order in many-body perturbation theory. Previous calculations [13–15, 25] beyond second order have focused on the inclusion of particle-particle ( $pp$ ) and hole-hole ( $hh$ ) ladder diagrams, whereas in the present work we compute, in addition to the third-order  $pp$  and  $hh$  diagrams, also the third-order particle-hole ( $ph$ ) diagram (without simplifying approximations), which has not been considered previously but is necessary for a consistent third-order calculation. The effects of the  $\text{N}^2\text{LO}$  3NF are included via a density-dependent two-body potential  $\bar{V}_{3N}$  that is added to the chiral  $\text{N}^3\text{LO}$  potential  $V_{2N}$ , and which is obtained by summing one nucleon over the non-interacting filled Fermi sea of nucleons [17, 26, 27].

The paper is organized as follows. In Sec. II, we briefly describe the features of the different chiral potentials employed and provide details about the renormalization procedure we have followed to choose the LECs of the 3NF terms  $V_{3N}^{1\pi}$  and  $V_{3N}^{\text{cont}}$ . In Sec. III, we outline the perturbative calculation of the energy per particle in symmetric nuclear matter that takes into account 3NF effects. Our results and conclusions are presented in Secs. IV and V, respectively.

## II. SCALE DEPENDENCE OF CHIRAL TWO- AND THREE-NUCLEON POTENTIALS

During the past two decades, chiral EFT has emerged as a powerful tool for describing hadronic interactions at low energy scales in a systematic and model-independent way (see Refs. [3, 28] for recent reviews). The separation of scales required to construct a useful EFT arises nat-

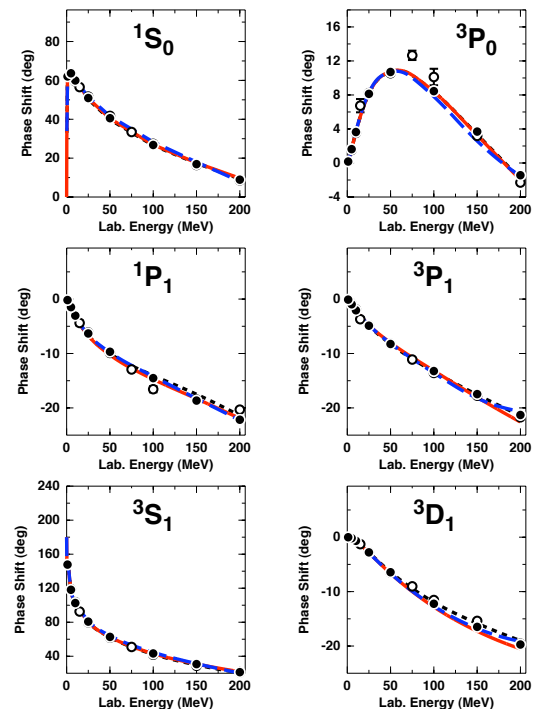


FIG. 1: (Color online) Neutron-proton phase shifts as predicted by chiral  $\text{N}^3\text{LO}$  potentials with different cutoff scale  $\Lambda$ . Solid (red) curve,  $\Lambda = 414$  MeV; dashed (blue) curve,  $\Lambda = 450$  MeV; and dotted (black) curve,  $\Lambda = 500$  MeV. Partial waves with total angular momentum  $J \leq 1$  are displayed. The solid dots and open circles are the results from the Nijmegen multi-energy  $np$  phase shift analysis [29] and the VPI/GWU single-energy  $np$  analysis SM99 [30], respectively.

urally in nuclear interactions from the pseudo-Goldstone boson nature of pions, which is associated with the spontaneous breaking of chiral symmetry and is responsible for the large difference between the light pion mass ( $m_\pi \simeq 135$  MeV) and the masses of the next lowest states in the meson spectrum, the  $\rho(770)$  and  $\omega(782)$ .

In normal nuclear many-body systems, the nuclear momenta are on the order of the pion mass, and therefore the systematic construction of chiral nuclear potentials is based on an expansion in powers of this soft scale ( $Q \sim m_\pi$ ) over the hard scale set by the typical hadron masses  $\Lambda_\chi \sim m_\rho \sim 1$  GeV, also known as the chiral-symmetry breaking scale. For this EFT to rise above the level of phenomenology, it must have a firm link with QCD. The link is established by having the EFT observe all relevant symmetries of the underlying theory, in particular, the broken chiral symmetry of low-energy QCD [31]. The past 15 years have seen great progress in applying ChPT to nuclear forces. As a result,  $NN$  potentials of high precision have been constructed, which

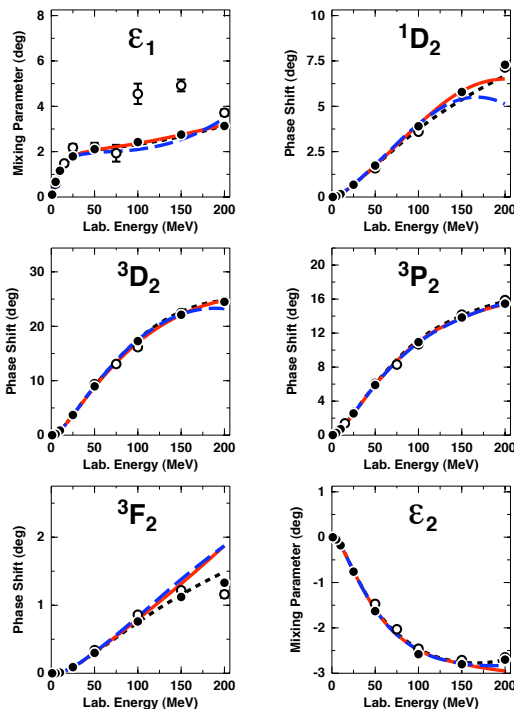


FIG. 2: (Color online) Same as Fig. 1, but for  $J = 2$  phase shifts and  $J \leq 2$  mixing parameters.

are based upon ChPT carried to N<sup>3</sup>LO.

Since ChPT is a low-momentum expansion, valid only for momenta  $Q < \Lambda_\chi$ , the potentials are multiplied with a regulator function, like, e. g., the one of Gaussian shape given in Eq. (1). In this investigation, we consider three N<sup>3</sup>LO  $NN$  potentials which differ by the cutoff scale  $\Lambda$  and the regulator function: (i)  $\Lambda = 414$  MeV using the regulator function Eq. (1) with  $n = 10$ , i.e., a smooth, but rather steep cutoff function is applied. This potential is very similar to the one with a sharp cutoff at 414 MeV published in Ref. [21]; however, a smooth version of the steep cutoff is more convenient in calculations of the three-body system. (ii)  $\Lambda = 450$  MeV, using the regulator function Eq. (1) with  $n = 3$ , which has been constructed for our study of Ref. [7] and the present investigation; (iii)  $\Lambda = 500$  MeV, using the regulator function Eq. (1) with  $n = 2$  for the  $2\pi$  exchange contributions [1]. All three potentials use the same (comprehensive) analytic expressions which can be found in Ref. [3]. Note that the Gaussian regulator function of Eq. (1) suppresses the potential also for  $Q < \Lambda$ , particularly for small  $n$ , which is the reason why we use  $n = 10$  for the case of the lowest cutoff of 414 MeV. Cutoff-independence is an important aspect of an EFT. In lower partial waves, the cutoff dependence of the  $NN$  phase shifts is counterbalanced by

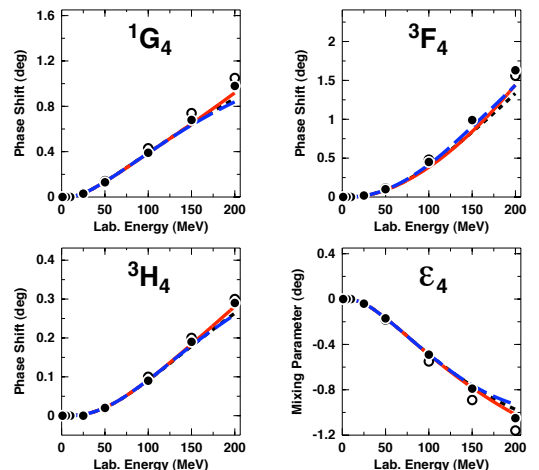


FIG. 3: (Color online) Same as Fig. 1, but for some representative peripheral partial waves.

an appropriate adjustment of the contact terms which, at N<sup>3</sup>LO, contribute in  $S$ ,  $P$ , and  $D$  waves. The extent to which cutoff independence can be achieved in lower partial waves is demonstrated in Figs. 1 and 2. In  $F$  and higher partial waves (where there are no  $NN$  contact terms) the LECs of the dimension-two  $\pi N$  Lagrangian can be used to obtain cutoff independence of the phase shift predictions, as shown in Fig. 3.

An important advantage of the EFT approach to nuclear forces is that it creates two- and many-body forces on an equal footing. The first non-vanishing 3NF occurs at N<sup>2</sup>LO. At this order, there are three 3NF topologies: the two-pion exchange (2PE), one-pion exchange (1PE) plus a 2N-contact interaction, and a pure 3N-contact interaction. These last two topologies are represented in Fig. 4.

The 2PE 3N-potential is given by

$$V_{3N}^{2\pi} = \left( \frac{g_A}{2f_\pi} \right)^2 \frac{1}{2} \sum_{i \neq j \neq k} \frac{(\vec{\sigma}_i \cdot \vec{q}_i)(\vec{\sigma}_j \cdot \vec{q}_j)}{(q_i^2 + m_\pi^2)(q_j^2 + m_\pi^2)} F_{ijk}^{ab} \tau_i^a \tau_j^b \quad (2)$$

with  $\vec{q}_i \equiv \vec{p}_i' - \vec{p}_i$ , where  $\vec{p}_i$  and  $\vec{p}_i'$  are the initial and

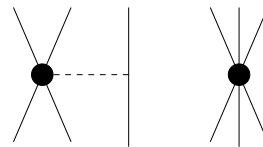


FIG. 4: The N<sup>2</sup>LO three-nucleon force contact interactions:  $V_{3N}^{1\pi}$  on the left and  $V_{3N}^{\text{cont}}$  on the right (see Eqs. (4) and (5), respectively).

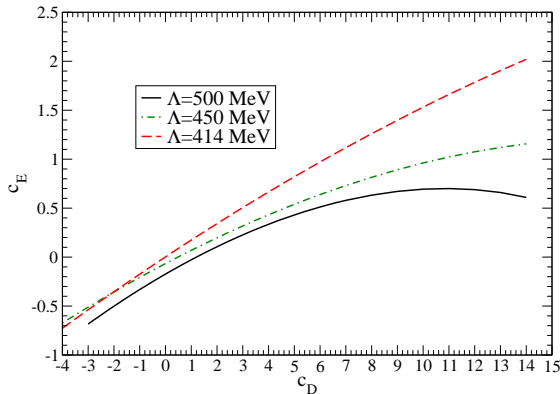


FIG. 5: (Color online)  $c_D$ - $c_E$  trajectories fitted to reproduce the experimental  ${}^3\text{H}$  and  ${}^3\text{He}$  binding energies. Solid (black) curve for  $\Lambda = 500$  MeV, dotted-dashed (green) curve for  $\Lambda = 450$  MeV, and dashed (red) curve for  $\Lambda = 414$  MeV.

final momenta of nucleon  $i$ , respectively, and

$$F_{ijk}^{ab} = \delta^{ab} \left[ -\frac{4c_1 m_\pi^2}{f_\pi^2} + \frac{2c_3}{f_\pi^2} \vec{q}_i \cdot \vec{q}_j \right] + \frac{c_4}{f_\pi^2} \sum_c \epsilon^{abc} \tau_k^c \vec{\sigma}_k \cdot [\vec{q}_i \times \vec{q}_j] \quad (3)$$

Note that the 2PE 3NF does not contain any new parameters, because the LECs  $c_1$ ,  $c_3$ , and  $c_4$  appear already in the 2PE 2NF. The 1PE contribution is

$$V_{3N}^{1\pi} = -\frac{c_D}{f_\pi^2 \Lambda_\chi} \frac{g_A}{8f_\pi^2} \sum_{i \neq j \neq k} \frac{\vec{\sigma}_j \cdot \vec{q}_j}{q_j^2 + m_\pi^2} (\vec{\tau}_i \cdot \vec{\tau}_j) (\vec{\sigma}_i \cdot \vec{q}_j) \quad (4)$$

and the 3N contact potential reads

$$V_{3N}^{\text{cont}} = \frac{c_E}{f_\pi^4 \Lambda_\chi} \frac{1}{2} \sum_{j \neq k} \vec{\tau}_j \cdot \vec{\tau}_k. \quad (5)$$

In the above, we use  $g_A = 1.29$ ,  $f_\pi = 92.4$  MeV,  $m_\pi = 138.04$  MeV, and  $\Lambda_\chi = 700$  MeV.

The last two 3NF terms involve the two new parameters  $c_D$  and  $c_E$ , which do not appear in the 2N problem. There are many ways to constrain these two parameters. The triton binding energy and the  $nd$  doublet scattering length  ${}^2a_{nd}$  or the  ${}^4\text{He}$  binding energy can be used. Given the known correlation between these observables, one may choose instead an optimal over-all fit of the properties of light nuclei [32]. However, recently a new procedure has been used to fix  $c_D$  and  $c_E$  [18–20]. Due to the consistency of interactions and currents in chiral EFT [18, 19], the LEC  $c_D$  that appears in  $V_{3N}^{1\pi}$  is also involved in the two-nucleon contact term in the  $NN$  axial current operator derived up to  $\text{N}^2\text{LO}$ . Therefore,  $c_D$  can be constrained using the accurate experimental value of one observable from weak processes involving two- or few-nucleon systems. Given the lack of accurate experimental values for weak observables in the two-body sector,

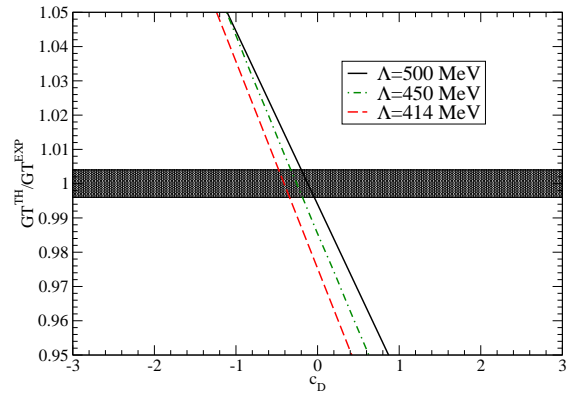


FIG. 6: (Color online) The ratio between the calculated GT value ( $\text{GT}^{\text{TH}}$ ) and the experimental one ( $\text{GT}^{\text{EXP}}$ ) as a function of the LEC  $c_D$ . Solid (black) curve for  $\Lambda = 500$  MeV, dotted-dashed (green) curve for  $\Lambda = 450$  MeV, and dashed (red) curve for  $\Lambda = 414$  MeV. The shaded stripe represents the experimental uncertainty.

the choice has been to use the triton  $\beta$ -decay half-life, in particular its Gamow-Teller (GT) component. This observable has been used already in a variety of studies to constrain the two-body axial current operator [20, 24, 33–35]. Therefore, we proceed here as in Ref. [20]: (i) We calculate the  ${}^3\text{H}$  and  ${}^3\text{He}$  wave functions with the hyperspherical harmonics method (see Ref. [36] for a review), using the chiral 2NF plus 3NF presented above for each cutoff parameter  $\Lambda$ . The corresponding set of LECs  $c_D$  and  $c_E$  are determined by fitting the  $A = 3$  experimental binding energies. The resulting trajectories are shown in Fig. 5. (ii) For each set of  $c_D$  and  $c_E$ , the  ${}^3\text{H}$  and  ${}^3\text{He}$  wave functions are used to calculate the GT matrix element. Comparison with the experimental value leads to a range of values for  $c_D$  for each cutoff parameter  $\Lambda$ , as shown in Fig. 6. Then, from Fig. 5, the corresponding range for  $c_E$  is determined. The values for  $c_D$  and  $c_E$  used in the present calculation are listed in Table I for each  $\Lambda$ . Note that the values of  $c_D$  and  $c_E$  for  $\Lambda = 500$  MeV are slightly different from those used in previous studies [20, 22, 24], but the GT matrix element is still reproduced within less than 1%.

At this point, a final remark is in order: the present fitting procedure employs  $\text{N}^3\text{LO}$   $NN$  interaction together with a 3NF derived at  $\text{N}^2\text{LO}$ , i.e., one chiral order lower. Furthermore, also the weak current operator is derived at  $\text{N}^2\text{LO}$ . To avoid this mismatch, it would be necessary to use  $\text{N}^3\text{LO}$  two- and three-nucleon interactions and currents. However, a derivation at  $\text{N}^3\text{LO}$  of the electroweak current would require the calculation of loop corrections, a task successfully performed for the electromagnetic [23], but not yet for the axial operators. Furthermore, the 3NF at  $\text{N}^3\text{LO}$  has been derived only recently [37, 38]

TABLE I: For the various chiral N<sup>3</sup>LO  $NN$  potentials used in the present investigation, we list the cutoff  $\Lambda$ , the type of regulator, the exponent  $n$  used in the regulator function [see Eq. (1)], the LECs of the dimension-two  $\pi N$  Lagrangian,  $c_i$  (in units of  $\text{GeV}^{-1}$ ), and the LECs  $c_D$  and  $c_E$  entering the three-nucleon potential.

Regulator type	Cutoff parameter $\Lambda$ (MeV)		
	414	450	500
Regulator type	Gaussian	Gaussian	Gaussian
$n$	10	3	2
$c_1$	-0.81	-0.81	-0.81
$c_2$	3.28	3.28	2.80
$c_3$	-3.00	-3.40	-3.20
$c_4$	3.40	3.40	5.40
$c_D$	-0.40	-0.24	0.0
$c_E$	-0.07	-0.11	-0.18

and, due to its complexity, only preliminary studies have been performed so far [16, 39, 40].

### III. NUCLEAR MATTER CALCULATIONS

We calculate the ground state energy (g.s.e.) per particle of infinite symmetric nuclear matter within the framework of many-body perturbation theory. More precisely, the g.s.e. is expressed as a sum of Goldstone diagrams up to third order.

As mentioned in Sec. I, the effects of the 3NF are taken into account via a density-dependent two-body potential  $\bar{V}_{3N}$ , that is added to the chiral N<sup>3</sup>LO potential  $V_{2N}$ . This potential is obtained by integrating one nucleon up to the Fermi momentum  $k_F$ , thus leading to a density-dependent two-nucleon interaction  $\bar{V}_{3N}(k_F)$ . At this time, analytic expressions for  $\bar{V}_{3N}$  [26, 27] has been derived only for the N<sup>2</sup>LO 3NF, which is the one we take into account in this work. We recall that to take care of the correct combinatorial factors of the normal-ordering at the two-body level of the 3NF, the matrix elements of  $\bar{V}_{3N}(k_F)$  have to be multiplied by a factor 1/3 in the first-order Hartree-Fock (HF) diagram, and by a factor 1/2 in the calculation of the HF single-particle energies [7, 17].

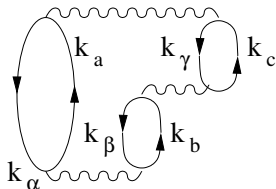


FIG. 7: Third-order ring diagram of the Goldstone expansion that we have included in our calculations with  $V_{2N}$  and  $\bar{V}_{3N}$  vertices. Latin-letter subscripts denote particle states, Greek-letter subscripts correspond to hole states.

We point out that in the present calculations we have summed the perturbation expansion up to third-order

in  $V_{2N} + \bar{V}_{3N}$ , in particular including the third-order particle-hole ( $ph$ ) diagram (see Fig. 7), which is also known as the third-order ring diagram [41]. This diagram has been taken into account neither in our previous paper [7], nor in other recent nuclear matter calculations which have employed chiral potentials within a perturbative approach [8, 9, 11, 15]. The analytic expressions of first-, second-, and third-order particle-particle ( $pp$ ) and hole-hole ( $hh$ ) contributions, together with the one of single-particle HF potential, have been already reported in Ref. [7]. The implicit expression of the third-order  $ph$  diagram can be found in Ref. [42], where also the explicit expressions for a potential without tensor and spin-orbit forces are reported.

The contributions of each diagram to the perturbation expansion obtained with the three chiral potentials for  $k_F = 1.3 \text{ fm}^{-1}$  without and with 3NF effects are given in Tables II and III, respectively. It is clear that the magnitude of the third-order  $ph$  diagram is large, bringing a relevant contribution to the third-order energy.

This is in line with the results shown in Ref. [16], where the neutron and nuclear EOS have been calculated within the coupled-cluster approach employing the chiral NNLO<sub>opt</sub> potential [43]. As a matter of fact, in [16] the inclusion of perturbative triples corrections in the coupled-cluster equations leads to corrections for the binding energy of about 1 MeV per nucleon, when including the 3NF in the normal-ordered two-body approximation. Furthermore, it is insightful to note that in Ref.[16] a significant contribution was found when going beyond the 3NF normal-ordered two-body approximation. With that in mind, we estimate the uncertainty of our perturbative result to be approximately 2 MeV.

In order to study the convergence properties of the perturbative expansion, it is useful to consider the [2/1] Padé approximant [44]

$$E_{[2/1]} = \mathcal{E}_0 + \mathcal{E}_1 + \frac{\mathcal{E}_2}{1 - \mathcal{E}_3/\mathcal{E}_2} , \quad (6)$$

$\mathcal{E}_i$  being the  $i$ th order energy contribution in the perturbative expansion of the g.s.e.. The Padé approximant is

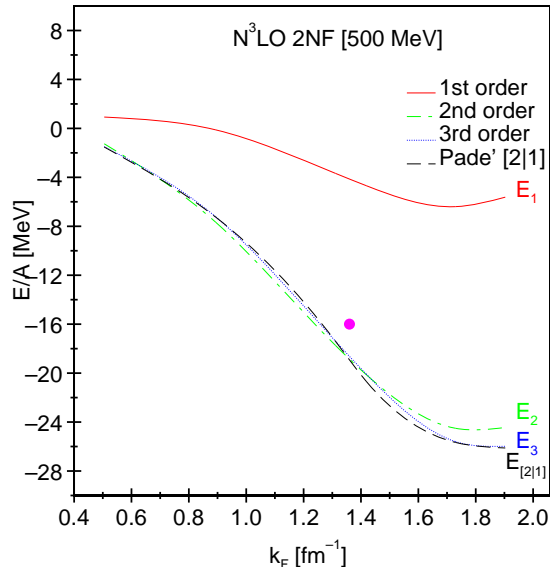


FIG. 8: (Color online) Nuclear matter energy per particle obtained from the  $N^3\text{LO}$  2NF with cutoff  $\Lambda = 500$  MeV. The first, second, and third order in the perturbative expansion and the Padé approximant [2|1] are shown as a function of the Fermi momentum  $k_F$ .

an estimate of the value to which the perturbative series may converge. Thus, in the following section we will perform a comparison between the third-order results and those obtained by means of the [2|1] Padé approximant, to obtain an indication of the size of the higher-order perturbative terms.

#### IV. RESULTS

In this section, we report the results of the calculation of the EOS of infinite symmetric nuclear matter in the framework of many-body perturbation theory. Since we include all contributions up to third order in the interaction, we are in a good position to study the convergence properties of the perturbative expansion.

We find that among the three chiral potentials under consideration, the least satisfactory perturbative behavior belongs to the chiral  $N^3\text{LO}$   $NN$  potential with  $\Lambda = 500$  MeV, whether the corresponding  $N^2\text{LO}$  3NF is included or not. This feature was already observed in our study of pure neutron matter [7] and is apparent in Figs. 8 and 9. In Fig. 8 we show the EOS as a function of the Fermi momentum  $k_F$ , calculated at various orders in the perturbative expansion applying the chiral  $N^3\text{LO}$   $NN$  potential with  $\Lambda = 500$  MeV. By inspection of the

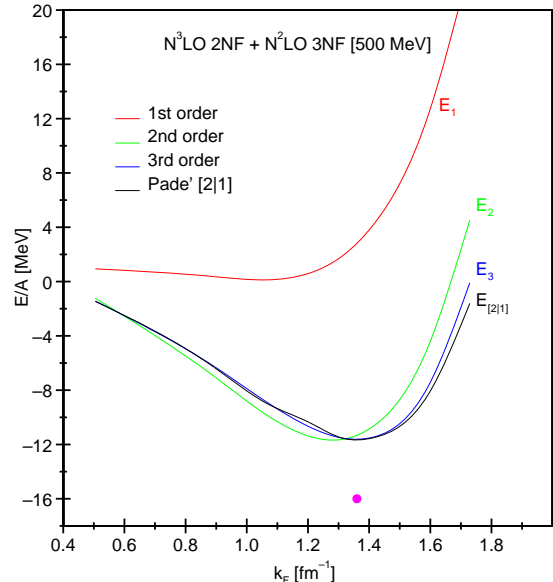


FIG. 9: (Color online) Same as in Fig. 8, but including the contribution of the  $N^2\text{LO}$  3NF.

figure, it can be seen that the energy per nucleon calculated at second order,  $E_2$ , does not differ much from the one computed at third order,  $E_3$ , for the whole range of Fermi momenta considered. The perturbative character is also indicated by the fact that the curve corresponding to  $E_3$  is almost indistinguishable from the [2|1] Padé approximant one.

Different considerations about the perturbative expansion have to be drawn when including the effects of 3NF. As a matter of fact, from inspection of Fig. 9, it can be seen that now the curve corresponding to  $E_3$  deviates from the one given by the [2|1] Padé approximant for  $k_F$  larger than  $1.6 \text{ fm}^{-1}$ , indicating a worsening of the perturbative behavior. On the other hand, using the other chiral potentials with lower cutoffs, the perturbative behavior is satisfactory at least up to  $k_F = 1.8 \text{ fm}^{-1}$ , as shown in Fig. 10 for  $\Lambda = 450$  MeV.

In Fig. 11 we display our predicted EOS obtained with chiral potentials that apply different regulator functions. We have added to each 2NF a 3NF whose LECs  $c_i$ , cutoff parameters, and regulator function are exactly the same as in the corresponding  $N^3\text{LO}$   $NN$  potential, see Table I, while the  $c_D$  and  $c_E$  LECs have been chosen such as to reproduce the observed  $A = 3$  binding energies and triton Gamow-Teller matrix element (see Sec. II). Our results have been obtained at third-order in the perturbative expansion, with and without taking into account 3NF effects.

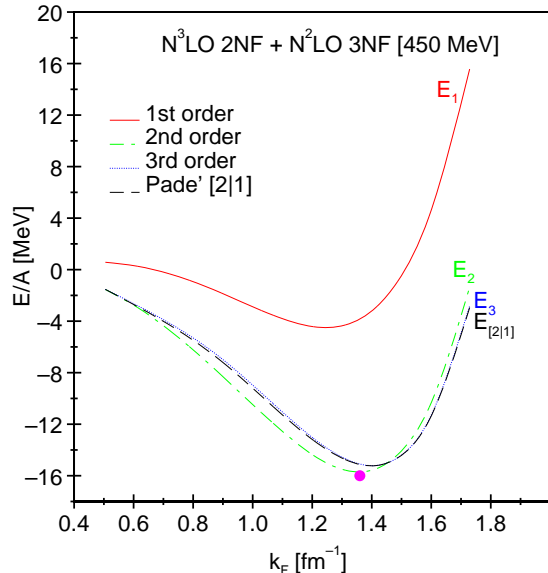


FIG. 10: (Color online) Same as Fig. 9, but for  $\Lambda = 450$  MeV.

The EOS calculated with 2NFs only and cutoffs  $\Lambda = 414, 450$  MeV are very close to each other, while the one corresponding to  $\Lambda = 500$  MeV is very different from the others. None of them show saturation, at least up to  $k_F = 1.9 \text{ fm}^{-1}$ . The differences between the predictions obtained with the two lower cutoffs on the one hand, and with the larger cutoff on the other, are not removed when including three-body effects. As a matter of fact, while the  $\Lambda = 414$  and  $450$  MeV EOS are nearly identical and show realistic saturation properties, the  $\Lambda = 500$  MeV EOS is considerably more repulsive. This is quite different from what we observed in pure neutron matter, where the inclusion of 3NF effects resulted in a (net) strong regulator-dependence reduction, with the predictions from the three potentials approaching one another.

In spite of the fact that the regulator dependence is not removed, the ability to obtain good saturation properties in a microscopic calculation, where the parameters are determined *via* the few-nucleon systems, should not be underestimated.

Another observation from this study is that the 3NF contribution to the energy per nucleon in symmetric nuclear matter is larger than in pure neutron matter [7] (about a factor of two at  $k_F = 1.35 \text{ fm}^{-1}$  for the  $\Lambda = 500$  MeV case). This may suggest that the weight of  $3p - 3h$  perturbative contributions induced by 3NF only (which are shown in Fig. 12 and are not included here but come into play at second order and beyond) could be non negligible.

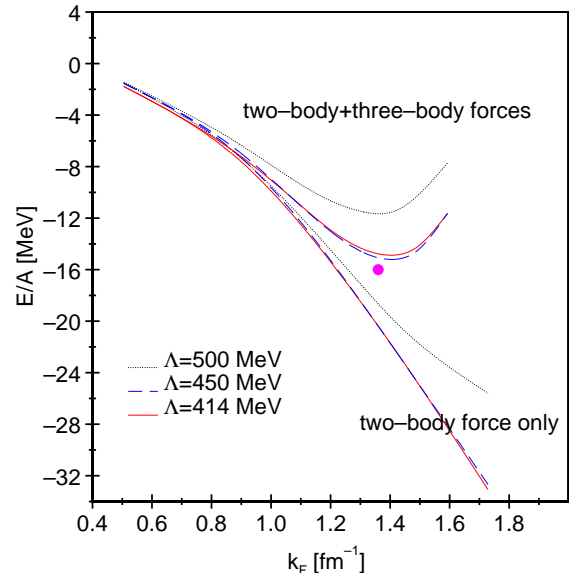


FIG. 11: (Color online) Results obtained for the g.s.e. per particle of infinite nuclear matter at third-order in perturbation theory for three sets of chiral interactions which differ by the cutoff  $\Lambda$ .

## V. CONCLUDING REMARKS AND OUTLOOK

In this paper we have studied the regulator dependence of many-body predictions of the EOS of symmetric nuclear matter, when employing chiral two- and three-nucleon potentials. This has been done within the framework of the perturbative Goldstone expansion, and using three different cutoffs and regulator functions for the derivation of the chiral potentials. We have adopted a consistent choice of the LECs and of the regulator functions for the two- and three-body components of the potential. In particular, the LECs  $c_D$  and  $c_E$  present in the 3NF have been fixed as to reproduce the experimental  $A = 3$  binding energies and Gamow-Teller matrix element in tritium  $\beta$ -decay.

Our calculations of the symmetric nuclear matter EOS show that, when employing chiral potentials with cutoffs  $\Lambda = 414$  and  $450$  MeV, the regulator independence provided by the renormalization procedure for the  $A \leq 3$  systems is preserved. We note again that these two potentials are found to exhibit good perturbative behavior. Moreover, the introduction of 3NF effects proves to be crucial for saturation and the predicted saturation properties are consistent with the empirical ones, within the uncertainty estimated on p.11. As mentioned above, this is a significant point, as it gives confidence in an *ab initio*

TABLE II: Contributions of each diagram to the perturbation expansion (in MeV) obtained with the three chiral potentials for  $k_F = 1.3 \text{ fm}^{-1}$  taking into account only 2NFs.

	Cutoff parameter $\Lambda$ (MeV)		
	414	450	500
HF contribution	-35.507	-32.786	-25.066
2nd order $pp$ diagram	-5.736	-8.551	-14.060
3rd order $pp$ diagram	0.017	-0.022	0.653
3rd order $hh$ diagram	-0.022	-0.021	-0.027
3rd order $ph$ diagram	1.040	1.200	-0.279

TABLE III: Same as in Table II, but including also 3NF effects.

	Cutoff parameter $\Lambda$ (MeV)		
	414	450	500
HF contribution	-28.792	-25.688	-19.503
2nd order $pp$ diagram	-7.388	-11.273	-13.511
3rd order $pp$ diagram	0.563	0.745	1.642
3rd order $hh$ diagram	-0.010	-0.008	-0.008
3rd order $ph$ diagram	0.581	0.152	-1.516

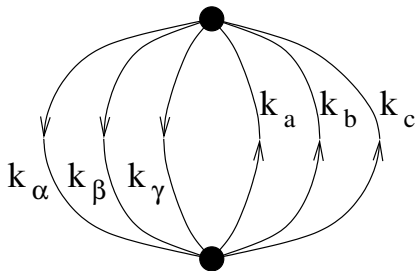


FIG. 12: Second-order Hugenholtz  $3p - 3h$  diagram of the Goldstone expansion with two 3NF vertices. Latin-letter subscripts denote particle states, Greek-letter subscripts correspond to hole states.

approach with two- and three-nucleon forces consistent with each other *and* with the properties of few-nucleon systems.

In a previous work [7], where the same topic has been studied for the pure neutron-matter EOS, we have found that the inclusion of 3NF effects is crucial to restore the above regulator independence also when employing the larger cutoff  $\Lambda = 500 \text{ MeV}$  potential. This is not the case, at least within a perturbative approach, in sym-

metric nuclear matter, where the  $\Lambda = 500 \text{ MeV}$  EOS is less attractive than the other two by 3 MeV per nucleon around  $k_F = 1.35 \text{ fm}^{-1}$ .

From the observation made in the previous section about the relative sizes of 3NF contributions in nuclear *vs.* neutron matter, we conclude that a calculation of the second-order  $3p - 3h$  diagram may shed light on whether the regulator dependence we have found is an issue with the perturbative expansion or with higher-order terms in ChPT, i.e. 3NF and 4NF at N<sup>3</sup>LO [45–48].

The inclusion of the diagram in Fig. 12 will be a topic of future studies, and may provide a better understanding of the application of chiral interactions in microscopic nuclear structure calculations.

### Acknowledgments

This work was supported in part by the U.S. Department of Energy under Grant No. DE-FG02-03ER41270 and No. DE-FG02-97ER-41014. We thank Norbert Kaiser for helpful discussions concerning the calculation of the third-order particle-hole diagram.

- 
- [1] D. R. Entem and R. Machleidt, Phys. Rev. C **68**, 041001(R) (2003).
  - [2] E. Epelbaum, W. Glöckle, and U.-G. Meissner, Nucl. Phys. A **747**, 362 (2005).
  - [3] R. Machleidt and D. R. Entem, Phys. Rep. **503**, 1 (2011).
  - [4] S. Weinberg, Phys. Lett. B **295**, 114 (1992).
  - [5] U. van Kolck, Phys. Rev. C **49**, 2932 (1994).
  - [6] L. Coraggio, A. Covello, A. Gargano, N. Itaco, and T. T. S. Kuo, Ann. Phys. **327**, 2125 (2002).
  - [7] L. Coraggio, J. W. Holt, N. Itaco, R. Machleidt, and F. Sammarruca, Phys. Rev. C **87**, 014322 (2013).
  - [8] F. Sammarruca, B. Chen, L. Coraggio, N. Itaco, and R. Machleidt, Phys. Rev. C **86**, 054317 (2012).
  - [9] I. Tews, T. Krüger, K. Hebeler, and A. Schwenk, Phys.

- Rev. Lett. **110**, 032504 (2013).
- [10] J. W. Holt, N. Kaiser, and W. Weise, Prog. Part. Nucl. Phys. **73**, 35 (2013).
- [11] T. Krüger, I. Tews, K. Hebeler, and A. Schwenk, Phys. Rev. C **88**, 025802 (2013).
- [12] A. Gezerlis, I. Tews, E. Epelbaum, S. Gandolfi, K. Hebeler, A. Nogga, and A. Schwenk, Phys. Rev. Lett. **111**, 032501 (2013).
- [13] A. Carbone, A. Polls, and A. Rios, Phys. Rev. C **88**, 044302 (2013).
- [14] G. Baardsen, A. Ekström, G. Hagen, and M. Hjorth-Jensen, Phys. Rev. C **88**, 054312 (2013).
- [15] M. Kohno, Phys. Rev. C **88**, 064005 (2013).
- [16] G. Hagen, T. Papenbrock, A. Ekström, K. A. Wendt, G. Baardsen, S. Gandolfi, M. Hjorth-Jensen, and C. J. Horowitz, Phys. Rev. C **89**, 014319 (2014).
- [17] K. Hebeler and A. Schwenk, Phys. Rev. C **82**, 014314 (2010).
- [18] A. Gärdestig and D. R. Phillips, Phys. Rev. Lett. **96**, 232301 (2006).
- [19] D. Gazit, Phys. Lett. B **666**, 472 (2008).
- [20] L. E. Marcucci, A. Kievsky, S. Rosati, R. Schiavilla, and M. Viviani, Phys. Rev. Lett. **108**, 052502 (2012).
- [21] L. Coraggio, A. Covello, A. Gargano, N. Itaco, T. T. S. Kuo, D. R. Entem, and R. Machleidt, Phys. Rev. C **75**, 024311 (2007).
- [22] M. Viviani, L. Girlanda, A. Kievsky, and L. E. Marcucci, Phys. Rev. Lett. **111**, 172302 (2013).
- [23] M. Piarulli, L. Girlanda, L. E. Marcucci, S. Pastore, R. Schiavilla, and M. Viviani, Phys. Rev. C **87**, 014006 (2013).
- [24] L. E. Marcucci, R. Schiavilla, and M. Viviani, Phys. Rev. Lett. **110**, 192503 (2013).
- [25] K. Hebeler, S. K. Bogner, R. J. Furnstahl, A. Nogga, and A. Schwenk, Phys. Rev. C **83**, 031301(R) (2011).
- [26] J. W. Holt, N. Kaiser, and W. Weise, Phys. Rev. C **79**, 054331 (2009).
- [27] J. W. Holt, N. Kaiser, and W. Weise, Phys. Rev. C **81**, 024002 (2010).
- [28] E. Epelbaum, H.-W. Hammer, and U.-G. Meißner, Rev. Mod. Phys. **81**, 1773 (2009).
- [29] V. G. J. Stoks, R. A. M. Klomp, M. C. M. Rentmeester, and J. J. de Swart, Phys. Rev. C **48**, 792 (1993).
- [30] R. A. Arndt, I. I. Strakovsky, and R. L. Workman, *Said scattering analysis interactive dial-in computer facility, george washington university (formerly virginia polytechnic institute), solution sm99 (summer 1999)*.
- [31] S. Weinberg, Physica **96A**, 327 (1979).
- [32] P. Navrátil, V. G. Gueorguiev, J. P. Vary, W. E. Ormand, and A. Nogga, Phys. Rev. Lett. **99**, 042501 (2007).
- [33] L. E. Marcucci, R. Schiavilla, M. Viviani, A. Kievsky, S. Rosati, and J. F. Beacom, Phys. Rev. C **63**, 015801 (2000).
- [34] T.-S. Park, L. E. Marcucci, R. Schiavilla, M. Viviani, A. Kievsky, S. Rosati, K. Kubodera, D.-P. Min, and M. Rho, Phys. Rev. C **67**, 055206 (2003).
- [35] L. E. Marcucci, M. Piarulli, M. Viviani, L. Girlanda, A. Kievsky, S. Rosati, and R. Schiavilla, Phys. Rev. C **83**, 014002 (2011).
- [36] A. Kievsky, S. Rosati, M. Viviani, L. E. Marcucci, and L. Girlanda, Journal of Physics G: Nuclear and Particle Physics **35**, 063101 (2008).
- [37] V. Bernard, E. Epelbaum, H. Krebs, and U.-G. Meissner, Phys. Rev. C **77**, 064004 (2008), 0712.1967.
- [38] V. Bernard, E. Epelbaum, H. Krebs, and U.-G. Meissner, Phys. Rev. C **84**, 054001 (2011), 1108.3816.
- [39] R. Skibinski, J. Golak, K. Topolnicki, H. Witala, E. Epelbaum, et al., Few Body Syst. **54**, 1315 (2013).
- [40] H. Witala, J. Golak, R. Skibinski, K. Topolnicki, H. Kamada, et al., Few Body Syst. **54**, 897 (2013).
- [41] H. A. Bethe, Phys. Rev. **138**, B804 (1965).
- [42] J. J. MacKenzie, Phys. Rev. **179**, 1002 (1969).
- [43] A. Ekström, G. Baardsen, C. Forssén, G. Hagen, M. Hjorth-Jensen, G. R. Jansen, R. Machleidt, W. Nazarewicz, T. Papenbrock, J. Sarich, et al., Phys. Rev. Lett. **110**, 192502 (2013).
- [44] G. A. Baker and J. L. Gammel, *The Padé Approximant in Theoretical Physics*, vol. 71 of *Mathematics in Science and Engineering* (Academic Press, New York, 1970).
- [45] E. Epelbaum, Phys. Lett. B **639**, 456 (2006).
- [46] S. Ishikawa and M. R. Robilotta, Phys. Rev. C **76**, 014006 (2007).
- [47] V. Bernard, E. Epelbaum, H. Krebs, and U.-G. Meißner, Phys. Rev. C **77**, 064004 (2008).
- [48] V. Bernard, E. Epelbaum, H. Krebs, and U.-G. Meißner, Phys. Rev. C **84**, 054001 (2011).